Impact of Relative Permeability Hysteresis and Capillary Pressure on Trapping Mechanisms During CO_2 Sequestration in Saline Aquifers

Aaditya Khanal[1]*, Md Irfan Khan[1]

[1]Jasper Department of Chemical Engineering, The University of Texas at Tyler

Abstract

This study aims to assess the impact of relative permeability hysteresis and capillary pressure on the long-term sequestration of CO_2 in sandstone aquifers. The scope includes evaluating the evolution of CO_2 trapping mechanisms, including dissolution, residual trapping, mineralization, and their variations over time. We employ a fine-scale numerical model based on a hypothetical siliciclastic reservoir to simulate 1000 years, including ten years of active injection followed by a monitoring phase. The effect of relative permeability hysteresis and capillary pressure on CO_2 trapping is analyzed for different time periods. The results reveal that capillary pressure is the most significant parameter that significantly increases the desired trapping mechanisms, such as residual, dissolution, and mineralization. At the end of 1000 years, a negligible fraction of CO_2 exists in the mobile phase when capillary pressure is included in the simulation. However, almost 50% of the injected CO_2 remains in the mobile phase when only relative permeability hysteresis is included in the model. Over the long term, dissolution trapping becomes the most dominant trapping mechanism, with mineralization contributing only a small fraction of sequestered CO_2. The impact of relative permeability hysteresis and capillary pressure on different trapping mechanisms is quantified, emphasizing their importance in predicting CO_2 behavior. This study provides critical aspects of CO_2 storage behavior and the impact of critical factors like relative permeability hysteresis and capillary pressure. The findings highlight the complexities of CO_2 trapping mechanisms over extended timeframes and demonstrate the importance of these factors in optimizing carbon capture and storage strategies. This research offers new information that can benefit geoscientists in improving the accuracy of CO_2 storage predictions and the safety of geological carbon sequestration.

Keywords: CO_2 Sequestration; Capillary Pressure; Relative Permeability Hysteresis; Dissolution Trapping

Introduction

Carbon dioxide (CO_2) accounted for approximately 79% of the total U.S. greenhouse gas (GHG) emissions in 2021 based on 100-year global warming potential [1]. The rise in GHG has increased the frequency and severity of climate-related disasters such as drought, flooding, storms, cyclones, wildfires, and winter storms. These natural disasters have resulted in significant measurable economic and societal damages. Despite a slight reduction in CO_2 emissions in 2020 due to the economic slowdown from the global pandemic, the CO_2 emissions rebounded to the

previous level in the subsequent years [2]. As the appetite for energy increases to fuel the economic output, there is a potential for a further rise in GHG in the atmosphere, resulting in irreversible damage to human society. In a sustainable development scenario proposed by the International Energy Agency (IEA) in which global CO_2 emissions from the energy sector fall to zero on a net basis by 2070, the majority of gain (~35%) is expected to come from improved energy efficiency [3]. The remaining improvements are expected from other areas, such as the shift to electrification and renewable fuels. CCUS (carbon capture utilization and storage) is projected to account for nearly 15% of the cumulative reduction in 2070 [4]. The contribution is expected to grow over time due to technological advancements and a fall in costs. Within CCUS, the geological sequestration of CO_2 into deep saline aquifers has garnered significant interest due to the potential of these geological formations to serve as massive storage volumes and long-term storage security [5,6].

Four main mechanisms play an important role in trapping the injected CO_2 in subsurface formations: hydrodynamic/structural, residual, solubility, and mineralization trapping. For long-term storage security, the latter three mechanisms are preferred as they reduce the mobility of the injected CO_2. Among the three mechanisms, mineralization plays only a minor role in long-term CO_2 storage, especially in siliciclastic formations, as it is not kinetically favored. Although dissolution trapping is the most dominant trapping mechanism in the long term [7,8], residual trapping traps the most significant fraction of CO_2 during the active injection and early part of the simulation phase [9]. During residual trapping, the injected CO_2 gets trapped as disconnected ganglia within the pore spaces. The continuous phase CO_2 snaps off and cannot flow as the saturation is below the critical saturation value within the trapped pores. The residually trapped CO_2 is immobilized throughout the reservoir, impeding its release into the atmosphere. The injected CO_2 begins to be residually trapped as soon as the injection starts, as the injected CO_2 rises through the reservoir due to the density gradient. The residual trapping occurs mainly due to the capillary forces and reservoir properties such as wettability and pore morphology/connectivity. Additionally, the capillary pressure and relative permeability hysteresis have a significant impact not only on residual trapping but also on other trapping mechanisms. Although the short-term impact of capillary pressure and relative permeability hysteresis has been investigated for residual trapping mechanisms, its long-term implications for dissolution, mineralization, and overall CO_2 sequestration are unclear, which is addressed in this paper.

Theory and Methodology

We use a compositional numerical reservoir simulator (CMG-GEM v. 2023.20) to build a 2D model for CO_2 storage in a deep saline aquifer. The simulator solves the fundamental mass and momentum transport in a closed system. The gas density is calculated with the Peng and Robinson equation (PR-EOS) [10], and the aqueous phase density and viscosity are calculated by Rowe and Chou [11] and Kestin et al. [12] correlation, respectively. The thermodynamic equilibrium of the gaseous and aqueous phases are modeled by the equality of the fugacity of the component in the gaseous and aqueous phases. The fugacity of a component in a gaseous phase is calculated using the PR-EOS [10]. Henry's law is used to calculate the fugacity of the components soluble in the aqueous phase. Henry's constant (H_i) is a function of pressure, temperature, and salinity. The variation of Henry's law constants based on reservoir pressure and temperature are modeled by using the Harvey correlation [13]. The molecular diffusion of CO_2 in brine is modeled using Fick's second law.

A homogeneous two-dimensional (2D) model with 4060 cartesian grid blocks (divided into 203x1x20 in I, J, and K directions, respectively) is created with a top-grid depth of 1700 m to represent a saline aquifer, as shown in **Fig. 1**. The grid block size in the I and K directions are optimized to use refined grid-blocks close to the wellbore using logarithmically spaced local grid refinement. We use no-flow boundaries at all four edges of the model.
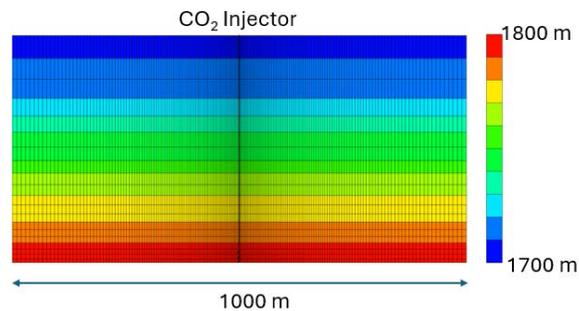
Fig. 1— Synthetic reservoir model used in the study.

The reservoir properties used for the simulation are:

Parameter	Units	Value
Grid cell number	-	4,060 (203x1x20)
Length	m	1,000
Height	m	100
Depth at the top	m	1,700
Porosity	fraction	0.15
Kv/Kh ratio	-	0.1
Permeability	mD	100
Pressure	Kpa	17,000
CO_2 injection rate	m³/day	100
Diffusion coefficient of CO_2 in brine	m².s⁻¹	2x10⁻⁵
Salinity	ppm	40,000
Injection rate	m³/day	100
Well bottom hole pressure (Maximum)	kPa	44,500

Table 1— Reservoir initial properties for the base case model

Chemical reactions occur between the minerals and aqueous components (heterogeneous reaction) and among the components within the aqueous phase (homogeneous reaction). The aqueous reactions are modeled as fast instantaneous equilibrium reactions, whereas the mineral reactions are modeled by using the transition state theory (TST) [14]. The solubility/dissolution of minerals is calculated based on the method described in Ngheim [15] using the solubility index. The following reactions and relevant inputs considered in the study are given in **Table 2**. Mineral reactive surface area (RSA) is a dynamic property; it changes with time and is significantly influenced by the heterogeneity, shapes, and complex contact interfaces [16]. This high degree of uncertainty of the mineral RSA is considered in our companion study [17], by simulating different cases using wide ranges of reported values in the literature. Results from our study showed that compared to other minerals, the RSA of quartz significantly influences the CO_2 mineralization process.

Reaction	Log-rate constant, $\log k_b$, $[mol/(m^2 s)]$ at $25^0 C$	Reactive surface area* $\hat{A}_j$, $[m^2/m^3]$	Activation energy, $E_{a\beta}$,) $[j/mol]$
$Quartz\ (SiO_2) =\ SiO_{2(aq)}$	-13.4	2,650	90,900
$K-feldspar\ (KAlSi_3O_8) + 4\ H^+$ $= 3\ SiO_2 + Al^{3+} + K^+ + 2\ H_2O$	-10.06	995,840	51,700
$Albite\ (NaAlSi_3O_8) + 4\ H^+$ $= 3\ SiO_2 + Al^{3+} + Na^+ + 2\ H_2O$	-10.16	1,021,800	16,600
$Calcite\ (CaCO_3) + H^+ =\ HCO_3^- + Ca^{2+}$	-0.3	2,710,000	14,400
$Dolomite\ (CaMg(CO_3)_2) + 2\ H^+$ $= 2\ HCO_3^- + Mg^{2+} + Ca^{2+}$	-3.19	284,000	56,700
$Siderite\ (FeCO_3) + H^+ =\ HCO_3^- + Fe^{2+}$	-10.097	3880.8	56,000
$Kaolinite\ (Al_2Si_2O_5(OH)_4) + 6\ H^+$ $= 2\ SiO_2 + 2\ Al^{3+} + 5\ H_2O$	-11.31	1,014,950	65,900

*RSA values reported in other units in cm²/g and m²/g converted to m²/m³

Table 2 — Mineral dissolution/precipitation reactions and kinetic parameters [18–21]

The initial volume fraction of the minerals [22] and brine chemistry [20,23] are given in **Table 3** and **Table 4**, respectively. The mineral volume fractions and brine chemistry represent the Mount Simon formation.

Mineral	Volume fraction (%)
Quartz	0.540
Albite	0.0176
K-feldspar	0.198
Calcite	0.00852
Dolomite	0.0244
Kaolinite	0.0261
Siderite	0.0350
Porosity	0.15
Total	1.00

Table 3— List of initial mineral volume fractions used for the simulation.

Ion	H^+	Ca^{2+}	Mg^{2+}	K^+	Na^+	Cl^-	Al^{3+}	Fe^{2+}	SiO_2
Concentration (mol/kg of H_2O)	$1.003e^{-6}$	0.47	0.099	0.036	1.8	9.034	$1e^{-5}$	0.0014	0.003

Table 4— Brine chemistry [15,24,25].

The relative permeability curves for water and gas were generated using the Brooks-Corey function [26]. In this study, the value of Corey exponents N_g and N_w is set to 4 and 9, respectively, and the value of $k_{r,g}(S_{wi})$ is assumed to be 0.95 [27]. The irreducible water saturation (S_{wi}) is assumed to be 0.22. As the aquifer is water wet, the liquid phase relative permeability curves are considered the same for drainage and imbibition processes [9,28]. However, the gas phase relative permeability experiences hysteresis, which was modeled by the Carlson model coupled with Land's model [29]. The maximum residual gas saturation due to hysteresis was selected as 0.21. The Brooks-Corey equation [26] is also used to obtain the capillary pressure for drainage with a capillary entry pressure of 4.6 kPa [27]. Capillary pressure hysteresis was not considered. **Fig. 2** shows the relative permeability with some of the scanning curves for K_{rg} and the capillary pressure curve used in the base case model.
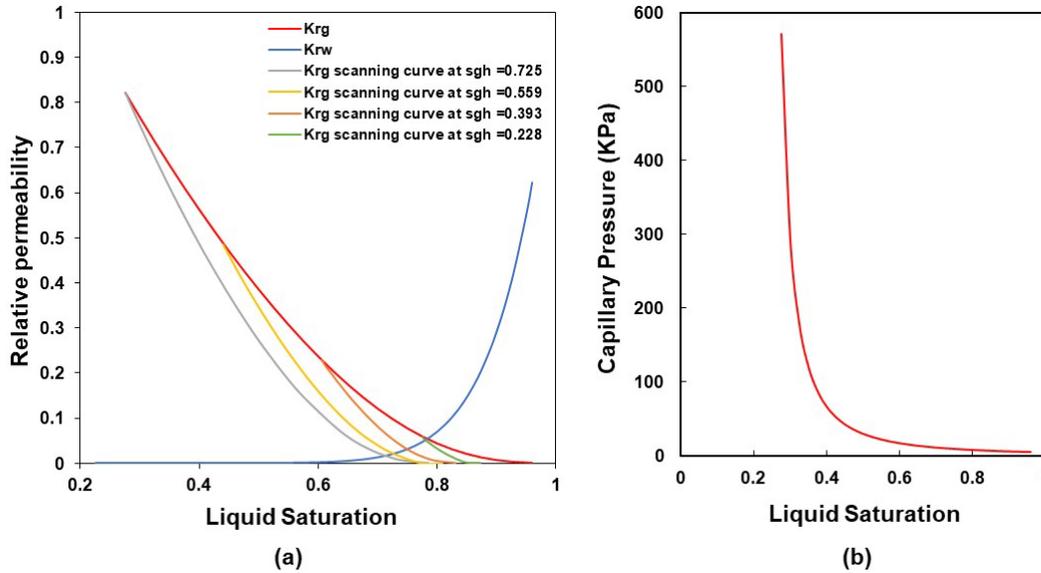
Fig. 2— (a) Relative permeability and scanning curve for drainage and imbibition and (b) Capillary pressure curve[17]**.**

Results and Discussion

This section presents the results from the geological model simulated for 1000 years, which includes a 10-year active simulation followed by the post-injection phase. The maximum bottom hole pressure constraint of 44,500 kPa is implemented for each run, which does not come into play for the injection rate used in the simulation. Hence, for each run, a fixed volume of CO_2 is injected, enabling fair comparison among all the cases. The simulation runs explored in this study are listed below:

Case	Description
1	Includes both relative permeability hysteresis (K_r) and capillary pressure
2	Ignores both relative permeability hysteresis (K_r) and capillary pressure
3	Includes capillary pressure but not relative permeability hysteresis
4	Includes relative permeability hysteresis but not capillary pressure

Table 5— List of simulations evaluated in this study

The total fraction of CO_2 by different mechanisms over the simulation period is illustrated in **Fig. 3**. During the active injection period of CO_2, the fraction of $ScCO_2$ in the reservoir rapidly increases. **Fig. 3a** shows up to 80% of the injected CO_2 exists in the supercritical phase for cases 2 and 4. We can also observe that the residually trapped CO_2 is at a minimum for case 2, which means that most of the injected gas exists in the mobile phase. This is because the relative permeability hysteresis included in cases 1 and 4 trap the injected CO_2 as an immobile phase. As soon as the injection is stopped, we observe a drastic increase in the fraction of residual CO_2 during the imbibition phase. Furthermore, the case with just relative permeability hysteresis (case 4) shows a higher fraction of residually trapped CO_2 compared to the case with just capillary pressure (case 3). However, **Fig. 3a** shows that the fraction of $ScCO_2$ in case 3 decreases significantly compared to all the other cases due to the significant increase in dissolution and mineralization. This is because case 3 has a larger fraction of mobile $ScCO_2$ than case 4 (or case 1), which comes in contact with fresh brine and gets trapped over larger areas due to capillary trapping. This results in faster dissolution compared to the case with residual trapping, which concentrates immobile CO_2 in a limited area, as will be seen later in **Fig. 4**. Other simulation and experimental studies [30,31] have also concluded that capillary pressure significantly enhances the dissolution of brine in reservoir conditions. The higher capillary pressure reduces gravity segregation, which results in a more homogeneous CO_2 plume, improving its dissolution. The increase in surface area between the immobilized CO_2 and brine also leads to improved mineralization, as observed in **Fig. 3d** and prior studies [30,31]. The results in this study also highlight that vertical permeability anisotropy has a significant impact on dissolution trapping. Our prior study showed that when there is no vertical permeability anisotropy, over 80% of the injected CO_2

may be trapped in the dissolved phase [17]. However, in this study, we only observe a maximum dissolution trapping of around 70% (case 3), as the reduced permeability in the vertical direction severely impedes the Rayleigh Taylor convective dissolution [32].

Although the relative hysteresis improves residual trapping, **Figs 3b-d** shows that it has a detrimental impact on dissolution and mineralization trapping. The residual CO_2 is immobilized in the pore spaces during the imbibition process and hence encounters limited contact with the brine, resulting in a decrease in both dissolution and mineralization trapping of CO_2. Overall, the least amount of the injected CO_2 exists in the mobile phase for case 3. We also observe that the fraction of CO_2 trapped by mineralization is negligible after 1000 years for each case. However, mineral precipitation and dissolution can significantly impact reservoir flow properties, as evaluated in other studies [17,33].

(a) Supercritical

(b) Residual

(c) Dissolved
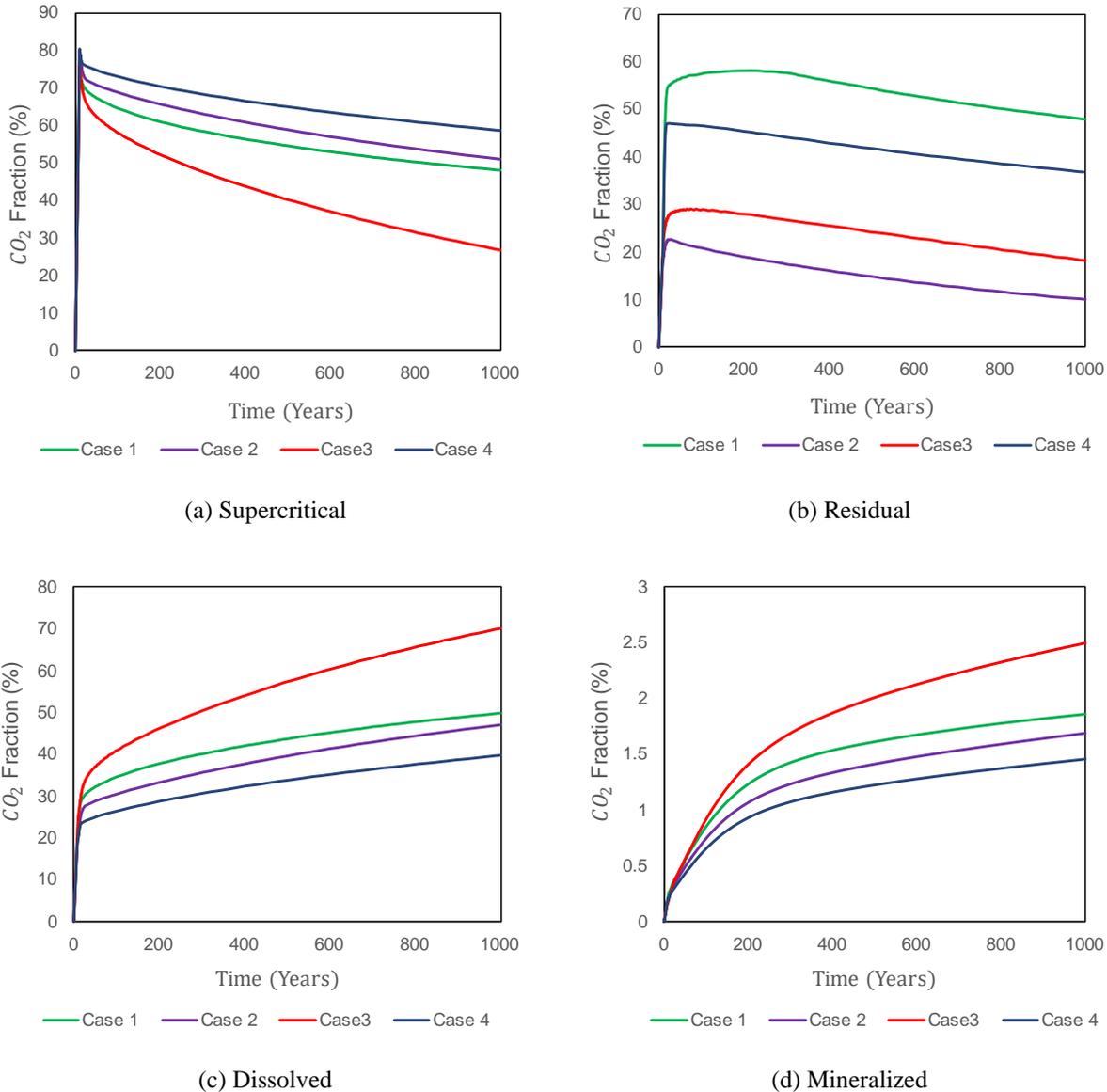
(d) Mineralized

Fig. 3— Fraction of CO_2 (specific phase/total injected) in (a) Supercritical, (b) Residually trapped, (c) Dissolved, and (d) Mineralized phases. The supercritical phase includes both mobile and residually trapped phases.

The results shown in **Fig. 3** can also be verified using the saturation plots after ten years, as shown in **Figs. 4a-b** for Cases 1 and 2. In cases where capillary forces are active (**Fig. 4a**), the gas saturation distribution reaches a maximum value of 0.34 around the perforation zone. The gas also does not reach the top of the reservoir during the active injection period. However, for case 2, which does not include capillary pressure and relative permeability hysteresis,

the highest gas saturation of 0.84 is observed around the perforation zones, and the injected CO_2 reaches the top of the reservoir. To further illustrate that case 2 has higher overall gas saturation, the scale of the saturation plot is constrained to 0.41 and highlighted in **Fig. 4c**. In order to isolate the effect of relative permeability hysteresis and capillary pressure, saturation plots of cases 3 and 4 (not shown) were compared to **Figs. 4a-b**, shown below. The saturation plot for case 1 was identical to case 3, whereas case 2 was identical to case 4. This result indicates that capillary pressure enhances the conversion of gas phase CO_2 to dissolved or mineralized form.
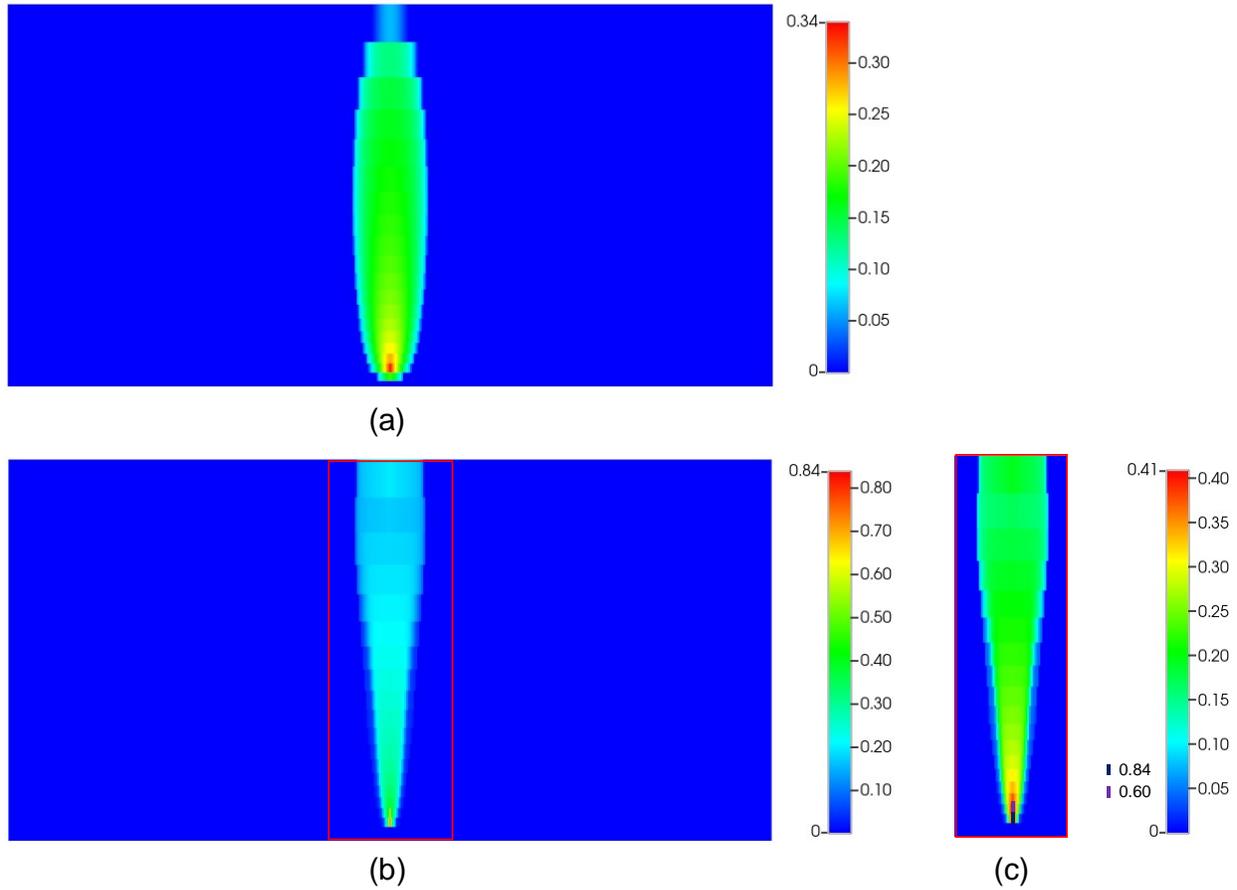
Fig. 3— Gas saturation after 10-years of active injection for (a) case 1 and (b) case 2. The magnified view of the wellbore shown in (b) after changing the upper scale is shown in (c).

As the bottom-hole pressure never reaches the imposed constraint, the well operates at a constant rate throughout the simulation period and reaches a pressure of slightly over 33,000 kPa. However, after the injection is stopped, we observe a rapid decline in the bottom-hole pressure for case 3, which can be attributed to the high rate of dissolution observed **(Fig. 3b)**. If only Henry's law is considered for dissolution, case 4, which has the highest pressure, it should have experienced the highest dissolution rate. The results here further reinforce the observation that capillary pressure has a significant implication for dissolution trapping for CO_2 sequestration in deep saline aquifers. Furthermore, we can also conclude that relative permeability hysteresis increases residual trapping but does not impact dissolution trapping.
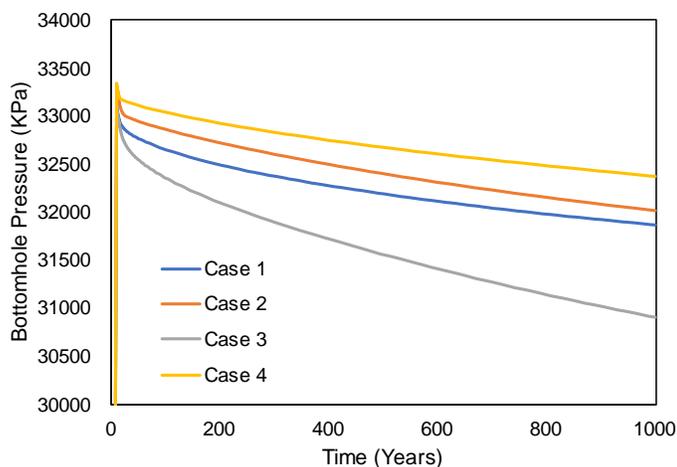
Fig. 5—The well bottom-hole pressure for each case after 1000 years of simulation.

Conclusions

This study evaluated the impact of relative permeability hysteresis and capillary pressure on different CO_2 trapping mechanisms. The key findings from this study are listed below:

  a) Capillary pressure is the most critical parameter that influences both dissolution and mineralization of CO_2 in saline aquifers (Figs. 3c-d).

  b) The relative permeability hysteresis increases the residually trapped CO_2, but it negatively impacts dissolution. This is because the relative permeability hysteresis traps a larger fraction of CO_2 within a limited area, limiting its contact with fresh brine (Fig. 4b).

  c) Dissolution and residual trapping are the most significant trapping mechanisms comprising the bulk of CO_2 trapped in saline aquifers.

  d) The low vertical permeability reduces the Rayleigh-Taylor convective dissolution, significantly reducing the fraction of CO_2 trapped by dissolution.

The findings in this study show that parameters used to model the capillary trapping and the relative permeability of a reservoir should be accurately characterized to estimate the amount of CO_2 trapped by various mechanisms.

Acknowledgments

References

[1]   USEPA, Inventory of U.S. Greenhouse Gas Emissions and Sinks: 1990-2020, 2022. https://www.epa.gov/ghgemissions/inventory-us-greenhouse-gas-emissions-and-sinks-1990-2020.

[2]   R. Jackson, Global carbon emissions from fossil fuels reached record high in 2023, Univ. Exet. Stanford Doerr Sch. Sustain. (2023). https://sustainability.stanford.edu/news/global-carbon-emissions-fossil-fuels-reached-record-high-2023#:~:text=The researchers estimate that the continuing a 10-year plateau.

[3]   IEA, CCUS in the Transition to Net-Zero Emissions [WWW Document]. Int. Energy Agency., (2023) 7823–7830. https://www.iea.org/reports/ccus-in-clean-energy-transitions/ccus-in-the-transition-to-net-zero-emissions.

[4]   IEA, CCUS in the Transition to Net-Zero Emissions [WWW Document]. Int. Energy Agency., (2023) 7823–7830.

[5]   S.M. Benson, D.R. Cole, CO2 Sequestration in Deep Sedimentary Formations, Elements. 4 (2008) 325–331. https://doi.org/10.2113/gselements.4.5.325.

[6]   S.J. Friedmann, Geological Carbon Dioxide Sequestration, Elements. 3 (2007) 179–184. https://doi.org/10.2113/gselements.3.3.179.

[7]   M.F. Shahriar, A. Khanal, Effect of Formation Heterogeneity on CO 2 Dissolution in Subsurface Porous Media, ACS Earth Sp. Chem. 7 (2023) 2073–2090. https://doi.org/10.1021/acsearthspacechem.3c00175.

[8]   A. Khanal, M.F. Shahriar, Physics-Based Proxy Modeling of CO2 Sequestration in Deep Saline Aquifers, Energies. 15 (2022) 4350. https://doi.org/10.3390/en15124350.

[9]   R. Juanes, E.J. Spiteri, F.M. Orr, M.J. Blunt, Impact of relative permeability hysteresis on geological CO 2 storage, Water Resour. Res. 42 (2006). https://doi.org/10.1029/2005WR004806.

[10]   D.-Y. Peng, D.B. Robinson, A New Two-Constant Equation of State, Ind. Eng. Chem. Fundam. 15 (1976) 59–64. https://doi.org/10.1021/i160057a011.

[11]   A.M. Rowe, J.C.S. Chou, Pressure-volume-temperature-concentration relation of aqueous sodium chloride solutions, J. Chem. Eng. Data. 15 (1970) 61–66. https://doi.org/10.1021/je60044a016.

[12]   J. Kestin, H.E. Khalifa, R.J. Correia, Tables of the dynamic and kinematic viscosity of aqueous NaCl solutions in the temperature range 20–150 °C and the pressure range 0.1–35 MPa, J. Phys. Chem. Ref. Data. 10 (1981) 71–88. https://doi.org/10.1063/1.555641.

[13]   A.H. Harvey, Semiempirical correlation for Henry's constants over large temperature ranges, AIChE J. 42 (1996) 1491–1494. https://doi.org/10.1002/aic.690420531.

[14]   A.C. Lasaga, Chemical kinetics of water-rock interactions, J. Geophys. Res. Solid Earth. 89 (1984) 4009–4025. https://doi.org/10.1029/JB089iB06p04009.

[15]   L. Nghiem, P. Sammon, J. Grabenstetter, H. Ohkuma, Modeling CO2 Storage in Aquifers with a Fully-Coupled Geochemical EOS Compositional Simulator, in: Proc. SPE/DOE Symp. Improv. Oil Recover., Society of Petroleum Engineers, 2004. https://doi.org/10.2523/89474-MS.

[16]   W. Jia, T. Xiao, Z. Wu, Z. Dai, B. McPherson, Impact of mineral reactive surface area on forecasting geological carbon sequestration in a co2-eor field, Energies. 14 (2021) 1–22. https://doi.org/10.3390/en14061608.

[17]   A. Khanal, M. Irfan Khan, M. Fahim Shahriar, Comprehensive Parametric Study of CO2 Sequestration in Deep Saline Aquifers, Chem. Eng. Sci. (2024) 119734. https://doi.org/10.1016/j.ces.2024.119734.

[18]   S.A. Carroll, W.W. McNab, Z. Dai, S.C. Torres, Reactivity of Mount Simon sandstone and the Eau Claire shale under CO 2 storage conditions, Environ. Sci. Technol. 47 (2013) 252–261. https://doi.org/10.1021/es301269k.

[19]   James L. Palandri and Yousif K. Kharaka, A Compilation of rate parameters of water-mineral interaction kinetics for application to geochemical modeling, California, 2004.

[20]   L. Zhang, Y. Soong, R. Dilmore, C. Lopano, Numerical simulation of porosity and permeability evolution of Mount Simon sandstone under geological carbon sequestration conditions, Chem. Geol. 403 (2015) 1–12. https://doi.org/10.1016/j.chemgeo.2015.03.014.

[21]   S.V. Golubev, P. Bénézeth, J. Schott, J.L. Dandurand, A. Castillo, Siderite dissolution kinetics in acidic aqueous solutions from 25 to 100 °C and 0 to 50 atm pCO2, Chem. Geol. 265 (2009) 13–19. https://doi.org/10.1016/j.chemgeo.2008.12.031.

[22]   D.M. Labotka, S. V. Panno, R.A. Locke, J.T. Freiburg, Isotopic and geochemical characterization of fossil brines of the Cambrian Mt. Simon Sandstone and Ironton-Galesville Formation from the Illinois Basin, USA, Geochim. Cosmochim. Acta. 165 (2015) 342–360. https://doi.org/10.1016/j.gca.2015.06.013.

[23]   G.P.D. De Silva, P.G. Ranjith, M.S.A. Perera, Geochemical aspects of CO2 sequestration in deep saline aquifers: A review, Fuel. 155 (2015) 128–143. https://doi.org/10.1016/j.fuel.2015.03.045.

[24]   R.A. Bauer, R. Will, S. E. Greenberg, S.G. Whittaker, Illinois Basin–Decatur Project, in: Geophys.

Geosequestration, Cambridge University Press, 2019: pp. 339–370.
https://doi.org/10.1017/9781316480724.020.

[25]   S. Luo, R. Xu, P. Jiang, Effect of reactive surface area of minerals on mineralization trapping of CO 2 in
        saline aquifers, Pet. Sci. 9 (2012) 400–407. https://doi.org/10.1007/s12182-012-0224-7.

[26]   Dullien and Francis AL, Porous media: fluid transport and pore structure, Academic Press Limited, 2012.

[27]   S.C.M. Krevor, R. Pini, L. Zuo, S.M. Benson, Relative permeability and trapping of CO 2 and water in
        sandstone rocks at reservoir conditions, Water Resour. Res. 48 (2012) 1–16.
        https://doi.org/10.1029/2011WR010859.

[28]   A. Kumar, R. Ozah, M. Noh, G.A. Pope, S. Bryant, K. Sepehrnoori, L.W. Lake, Reservoir Simulation of
        CO2 Storage in Deep Saline Aquifers, SPE J. 10 (2005) 336–348. https://doi.org/10.2118/89343-PA.

[29]   C.S. Land, Calculation of Imbibition Relative Permeability for Two- and Three-Phase Flow From Rock
        Properties, Soc. Pet. Eng. J. 8 (1968) 149–156. https://doi.org/10.2118/1942-PA.

[30]   H. Alkan, Y. Cinar, E.B. Ülker, Impact of Capillary Pressure, Salinity and In situ Conditions on CO2
        Injection into Saline Aquifers, Transp. Porous Media. 84 (2010) 799–819. https://doi.org/10.1007/s11242-
        010-9541-8.

[31]   S. Benson, S.; Pini , R.;Reynolds, C.; and Krevor, Relative permeability analyses to describe multi-phase
        flow in CO2storage reservoirs, 2013.

[32]   M.F. Shahriar, A. Khanal, Fundamental investigation of reactive-convective transport: Implications for long-
        term carbon dioxide (CO2) sequestration, Int. J. Greenh. Gas Control. 127 (2023) 103916.
        https://doi.org/10.1016/j.ijggc.2023.103916.

[33]   M.V.B. Machado, M. Delshad, K. Sepehrnoori, Injectivity assessment for CCS field-scale projects with
        considerations of salt deposition, mineral dissolution, fines migration, hydrate formation, and non-Darcy
        flow, Fuel. 353 (2023) 129148. https://doi.org/10.1016/j.fuel.2023.129148.